IBRACON Structures and Materials Journal
Revista IBRACON de Estruturas e Materiais
ISSN 1983-4195 ismj.org

ORIGINAL ARTICLE

Interference effects on wind loads as prescribed by codes and standards: can they be generalized?

Efeitos de interferência nas cargas do vento prescritos por códigos e normas: eles podem ser generalizados?

Thiarly Feitosa Afonso de Lavôr[a]
José Luis Vital de Brito[b]
Acir Mércio Loredo-Souza[c]

[a]Centro Universitário Santa Maria, Cajazeiras, PB, Brasil
[b]Universidade de Brasília – UnB, Departamento de Engenharia Civil e Ambiental, Brasília, DF, Brasil
[c]Universidade Federal do Rio Grande do Sul – UFRGS, Laboratório de Aerodinâmica das Construções, Porto Alegre, RS, Brasil

Received 3 August 2023
Revised 29 November 2023
Accepted 9 January 2024

Abstract: Understanding and quantifying the effects of aerodynamic interference is fundamental to designing safe and efficient buildings; however, there is a complexity in this phenomenon that characterizes it as the greatest challenge of wind engineering and thus limits improving design guidelines in a normative way. Therefore, this study investigated the impacts of building interference on wind-induced loads on a tall building through wind tunnel tests conducted using the synchronous pressure measurement technique. This impact was quantified using the interference factors (IFs) on the along-wind, across-wind and torsional force coefficients, which were mapped considering different wind angles, relative positions and number of buildings, in addition to the terrain roughness. It was observed that the protection effect in a static analysis is a dominant phenomenon in most studied scenarios when there is wind interference. The largest extension of the amplification zones occurred in scenarios in which the wind blew against the smallest facade of the analyzed building and the largest facade of the interfering building, where the coefficient of torsional moment was more sensitive to changes in wind turbulence.

Keywords: interference effects, wind tunnel, tall buildings, static analysis, design standards.

Resumo: Compreender e quantificar os efeitos de interferência aerodinâmica é fundamental para projetar edifícios seguros e eficientes, no entanto, há uma complexidade nesse fenômeno que o caracteriza como o maior desafio da engenharia do vento e, por tanto, limita o aprimoramento das diretrizes de projeto de maneira normativa. Logo, essa pesquisa investigou o impacto da interferência de edificações nas cargas induzidas pelo vento em um edifício alto, através de testes em túnel de vento conduzidos utilizando a técnica de medição de pressão síncrona. Esse impacto foi quantificado por meio dos fatores de interferência (FIs) nos coeficientes da força longitudinal, transversal e torcional, os quais foram mapeados considerando diferentes ângulos de vento, posições relativas e quantidade dos edifícios, além da rugosidade do terreno. Observou-se que o efeito de proteção em uma análise estática é um fenômeno dominante na maioria dos cenários estudados quando há interferência do vento. A maior extensão das zonas de amplificação ocorreu nos cenários em que o vento incidiu na menor fachada do edifício analisado e na maior fachada do edifício interferente, onde o coeficiente do momento torcional mostrou-se mais sensível às mudanças de turbulência do escoamento do vento.

Palavras-chave: efeitos de interferência, túnel de vento, edifícios altos, análise estática, normas de projeto.

How to cite: T. F. A. Lavôr, J. L. V. Brito, and A. M. Loredo-Souza, "Interference effects on wind loads as prescribed by codes and standards: can they be generalized?", *Rev. IBRACON Estrut. Mater.*, vol. 17, no. 6, e17607, 2024, https://doi.org/10.1590/S1983-41952024000600007

Corresponding author: Thiarly Feitosa Afonso de Lavôr. E-mail: thiarlycz@hotmail.com
Financial support: None.
Conflict of interest: Nothing to declare.
Data Availability: Due to the nature of this research, participants of this study did not agree for their data to be shared publicly, so supporting data are not available.

1 INTRODUCTION

The construction of increasingly taller and more flexible buildings has led to the development of more severe aerodynamic phenomena, including so-called interference effects (IEs). These effects arise due to changes in wind load caused by buildings or obstacles immersed in its flow, which can be amplified or reduced. Understanding and quantifying IEs is fundamental to designing safe and efficient buildings; however, there is a complexity in this phenomenon that characterizes it as the greatest challenge of wind engineering and thus limits improving design guidelines in a normative way.

Given this difficulty, several studies have sought to understand the interference effects through variations in parameters such as the number of buildings and their locations, characteristics of the simulated wind and its direction of incidence, terrain roughness, relative dimensions of the buildings and their shapes, and even natural frequencies, mode shapes, Scruton and Strouhal numbers, as seen in Saunders and Melbourne [1], Sykes [2], Blessmann [3], Bailey and Kwok [4], Kareem [5], Taniike [6], Gu et al. [7], Fang et al. [8], Wang et al. [9], Lo et al. [10], Reis et al. [11] and Wang et al. [12].

To facilitate identifying the influence that the involved parameters have on changes in aerodynamic loads it is common to use maps of the interference effects in a given territorial extension. These maps are presented in the Indian and Japanese standards and in the comments of the Chinese standard, in addition to being present in studies by major researchers on the subject.

In Xie and Gu [13], a slight superiority of the protective effects was observed in situations with one and two interfering buildings on smoother turbulence, as well as higher amplification of the interference effects on rougher terrain. According to the presented maps of the interference effects, there was a reduction in wind loads in regions with $x/b < 10$ and $y/b < 2$, where x and y are the longitudinal and transversal coordinates of the wind, respectively, and b is the width of the building. Amplified interference effects occurred, generally in regions of the maps with $y/b > 2$.

In a static study by Mara et al. [14], reductions in the mean along-wind moments and amplifications (5%) in the RMS along-wind moments were identified in the presence of the interfering buildings in positions, generally with $y/d > 2.5$, where d is the width of the building, in both tested terrains. The across-wind and torsional responses in RMS values, according to the presented maps, had important amplifications in regions with $y/d > 1$ and, respectively, at $x/d = 5$ and $x/d = 7$, reaching 40% in the open country exposure. However, these values decreased significantly in urban terrains, reaching 15% amplification in the RMS across-wind moments and 10% in the RMS torsion moments.

Kim et al. [15] found that interference between buildings notably affects the along-wind base moment when the height ratio between the interfering building and the principal building is equal to 1 and 1.5. In addition, when a taller interfering building was located at coordinates $(x/b, y/b) = (1.5, 1)$, the mean and fluctuating along-wind and across-wind loads increased by approximately 30%.

According to Lavôr et al. [16], the highest amplifications in the along-wind, across-wind and torsional static force coefficients occurred when the incident wind was against the smaller facade of the principal building and against the larger facade of the interfering buildings, when they were positioned in oblique regions to the principal building, reaching 20%, 100% and 80%, respectively.

In this work, analyses of IEs on the resisted wind loading of a tall building in the presence of the interfering buildings with similar dimensions are presented. Wind tunnel tests were performed using the technique of synchronous high-frequency pressure measurement. The IEs in the mean along-wind, RMS across-wind and RMS torsion of global aerodynamic forces were analyzed and quantified based on interference factors by considering several parameters in the tests, such as the terrain roughness, the angles of incidence of the wind, the distances between the buildings and the number of structures involved. The major interference factors identified were represented in contour maps and compared to normative prescriptions.

2 EXPERIMENTAL PROGRAM

2.1 Experimental configuration

The experiments were performed in the closed-circuit atmospheric boundary layer wind tunnel of the Federal University of Rio Grande do Sul, located in Brazil. The test section of the tunnel used in this study was 130 cm wide, 90 cm high and 932 cm long. The natural wind profile was simulated using devices such as triangular fins, a hollow horizontal bar and roughness blocks (Figure 1), which were represented by the mean velocity and the turbulence intensity profiles determined, respectively, by the power law (Equation 1) and Equation 2.

(a) $p = 0.11$ (b) $p = 0.23$

Figure 1. Devices used to simulate natural wind profile.

$$\bar{V}(z) = V_0 \left(\frac{z}{z_0} \right)^p \tag{1}$$

where $\bar{V}(z)$ is the mean wind velocity along the height z of the test section of the tunnel; V_0 is the mean wind velocity at a reference height z_0; and p is the exponent of the potential law, which relates the mean velocity profile to the terrain categories. The values used for these exponents were 0.11 and 0.23, corresponding, respectively, to Category I and a range between Categories III and IV of the Brazilian standard NBR 6123 [17].

$$\mathrm{I}(z) = \frac{\sigma_V(z)}{\bar{V}(z)} \tag{2}$$

where $I(z)$ and $\sigma_V(z)$ is the turbulence intensity and the standard deviation of the velocity fluctuations, respectively, along the height z of the test section of the tunnel.

The flow characteristics along the height were analyzed considering the mean velocity profile, the turbulence intensity and the normalized longitudinal velocity fluctuations spectrum as a function of reduced frequency, as shown in Figure 2. The mean reference velocity is measured at a height of z_0 = 450 mm of the tunnel, reaching values of approximately V_0 = 25 m/s.

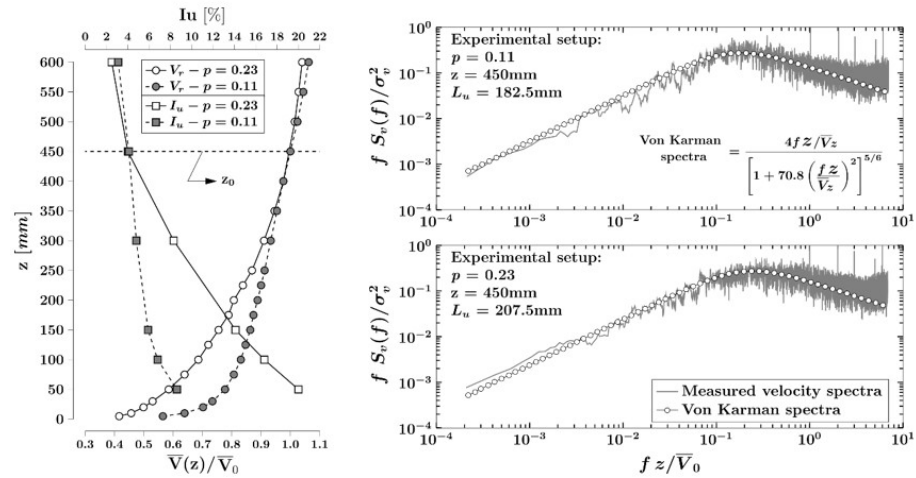

(a) Mean velocity and turbulence profiles (b) Longitudinal velocity fluctuations spectrum

Figure 2. Simulated natural wind parameters.

The tunnel analysis system uses an electronic sensor from Scanivalve Corp, specifically the ZOC33 model. This sensor consists of 6 sets of modules, each with 64 channels, allowing high-frequency data capture with a maximum acquisition rate of 20 kHz. The inaccuracy associated with this sensor is 0.12%. For the purpose of this research, the sensor recorded a total of P = 8192 pressure measurements per channel during a period of T = 16 s, resulting in an acquisition rate of 512 Hz.

The modules were connected to the standard building model, available in the wind tunnel for research, by measuring taps. The model itself was built with acrylic plates with a height of 450 mm and a section with dimensions of 112.5 × 75 mm. The length scale used was 1:406.4. The measurement points were distributed around the perimeter of the model in 10 different levels, with each level having 28 measurement points (7 points per facade). In all, N = 280 pressure taps were used, distributed as illustrated in Figure 3a, with dimensions corresponding to full scale.

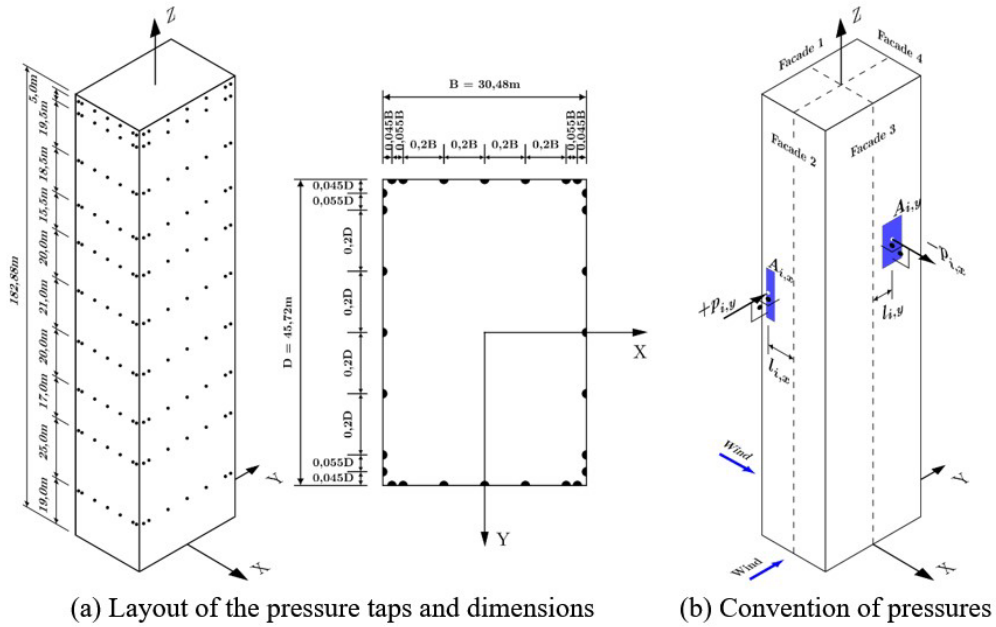

Figure 3. Characteristics of the analyzed model building.

2.2 Interfering building conditions

The interference effects were analyzed considering the position and number of interfering buildings with the same dimensions as the principal building, identified as “C” in Figure 4. The interfering buildings were systematically positioned to the upstream side of the principal building in order to evaluate positions which had not yet been analyzed by previous research, and were classified as variables “V”, fixed “D1” and fixed “D2”.

The grid arrangements of the relative positions of the interfering buildings can be classified into three groups of experiments: 1) (1I) - 1 interfering building “V” varying its position in 23 points; 2) (2I-D1) - 2 interfering buildings, 1 “V” varying its position in 23 points and the “D1” fixed; and 3) (2I-D2) - 2 interfering buildings, 1 “V” varying its position in 23 points and the “D2” fixed. The variation of the interfering buildings “V” is indicated in the grids in Figure 4 by small circles, referring to the geometric center of the building. The coordinate Y/B = 0 represents the centerline of the wind tunnel, where B is the smaller side of the cross-section of the principal building.

In addition to the distance and number of buildings, the influence of the direction of wind incidence was investigated, defining four sets of relative rotations between the principal building and the interfering one, as illustrated in Figure 5. The sets were as follows: 1) (C0V0) – Principal and interfering buildings at 0° rotation; 2) (C0V90) – Principal building at 0° rotation and interfering building at 90° rotation; 3) (C90V0) – Principal building at 90° rotation and interfering building at 0° rotation; and 4) (C90I90) – Principal and interfering buildings at 90° rotation. The fixed interfering building (“D1” or “D2”), when present, followed the same rotation as the variable interfering building.

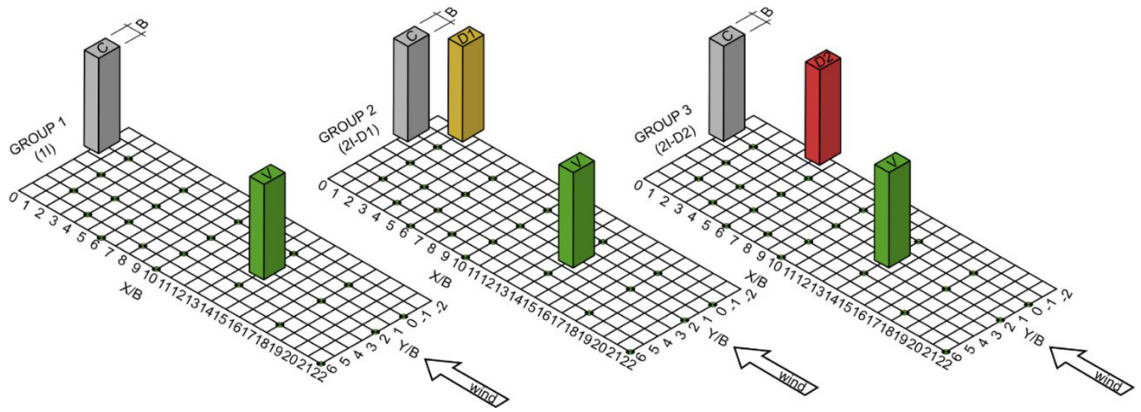

Figure 4. Groups and grids of interference positions.

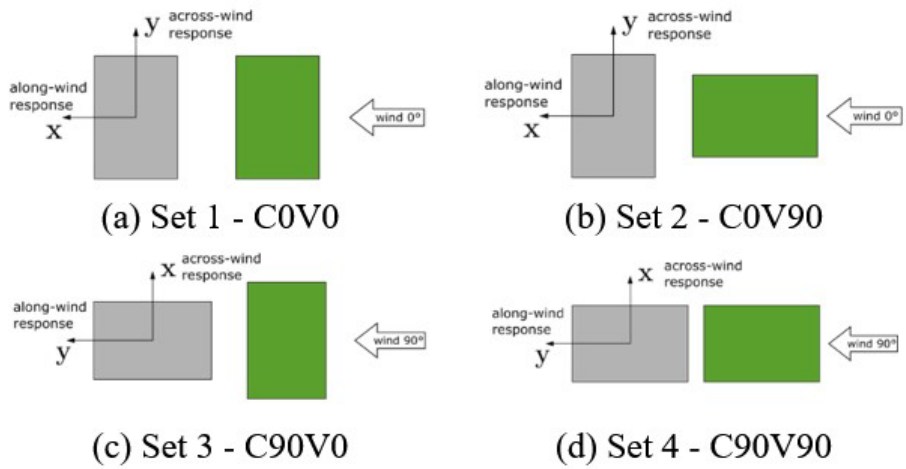

Figure 5. Sets of relative rotation between buildings.

Angles of 0° or 90° were assigned to all models when their larger or smaller sides were perpendicular to the direction of the incident wind, respectively. Although other wind incidence angles are relevant in the analysis of interference effects, as evidenced by Kim et al. [15] and Hui et al. [18], in this study, this was limited to the mentioned angles, since these are the ones that most standards and codes use in their approaches.

2.3 Data processing

The time history of the total wind load on the facades of the axis analyzed for the two directions of incidence, as well as the torsional moment at the base, were calculated from the integration of the measured pressures, according to the following Equations 3 and 4.

$$F_{axis,\alpha}(t) = \sum_{i=1}^{n_f} P_{i,\alpha}(t) \cdot A_i \tag{3}$$

$$M_{T,\alpha}(t) = \sum_{i=1}^{n_S} P_{i,\alpha}(t) \cdot A_i \cdot l_i \tag{4}$$

where n_f is the number of pressure taps on the facades of the axis considered and n_S is the total number of pressure taps on the surface of the model. Considering the i^{th} pressure tap, A_i is its tributary area, and $P_{i,\alpha}(t)$ is the instantaneous pressure measured. Where α is the angle of the wind incidence and l_i is the perpendicular distance between the

measurement point and the torsion center of the building, as shown in Figure 3b. The tributary areas are associated with direction cosines, in order to consider its orientation in relation to the coordinate axes; however, it has been omitted from Equations 3 and 4 due to the orthogonal angles of wind incidence used in this research.

The most practical and widely used way to analyze a temporal sequence of wind pressures is through aerodynamic coefficients, which were determined here as follows by Equations 5 and 6.

$$C_F(t) = \frac{F_{axis,\alpha}(t)}{q \cdot B \cdot H} \tag{5}$$

$$C_T(t) = \frac{M_{T,\alpha}(t)}{q \cdot B \cdot D \cdot H} \tag{6}$$

where $C_F(t)$ and $C_T(t)$ represent the coefficients of the total instantaneous force and the torsion moment, respectively. B and D correspond to the smaller and the larger dimension of the principal building cross-section, respectively, and H to its height. In addition, q refers to the dynamic pressure, which is measured at the top of the building model at the time of the test, corrected in some cases with two interfering buildings that had a blocking factor of approximately 10%.

After calculating the mean coefficient for the along-wind force and RMS for the across-wind force and for the torsional moment in all tested cases, it was possible to estimate the interference effects. These effects are often expressed by interference factors (IFs), defined below, which quantifies the wind load acting against a building changed due to the presence of upstream or downstream interfering buildings.

$$IF = \frac{C \text{ in the presence of the interference building}}{C \text{ in the isolated principal building case}} \tag{7}$$

where C represents the aerodynamic coefficient analyzed in the principal building.

3 RESULTS AND DISCUSSION

3.1 Mapping of interference effects

With the aerodynamic coefficients calculated from the experimental data, contour plots were generated using the Kriging regression method, taking into account the interference factors (IFs). To simplify the maps, the results for the coordinates of the negative Y/B axis can be considered equivalent to the results shown in the positive Y/B axis when the experimental cases of the building arrangements are mirrored, and for this reason, these results were not included in the graphs. The results for the negative X/B axis have different values than the positive X/B axis and were also not presented because there were no experimental data at these positions. The contour plots presented are specific for the roughness of p = 0.11, as illustrated in Figures 6-11, and consider three groups of interfering buildings and the four relative rotations of the buildings, as shown in Figures 4 and 5, respectively.

3.1.1 Along-wind force coefficients

Considering the principal building at 0° (C0), the contour plots showed a significant area of protection (or shielding effect) caused by the interfering building, especially when there are two upstream buildings, as shown in Figure 6. However, amplification effects were also observed, present from the coordinates Y/B = 4 and along the X/B axis in cases where there is a single upstream building, with more intensity in the scenario with C0V0, as illustrated in Figure 6a, in relation to the scenario with interfering building V90, as shown in Figure 6d.

Hui et al. [19] showed that the interference factors were slightly higher when the wind was perpendicular to the larger facade of the interfering building compared to the wind on the smaller facade of the upstream building.

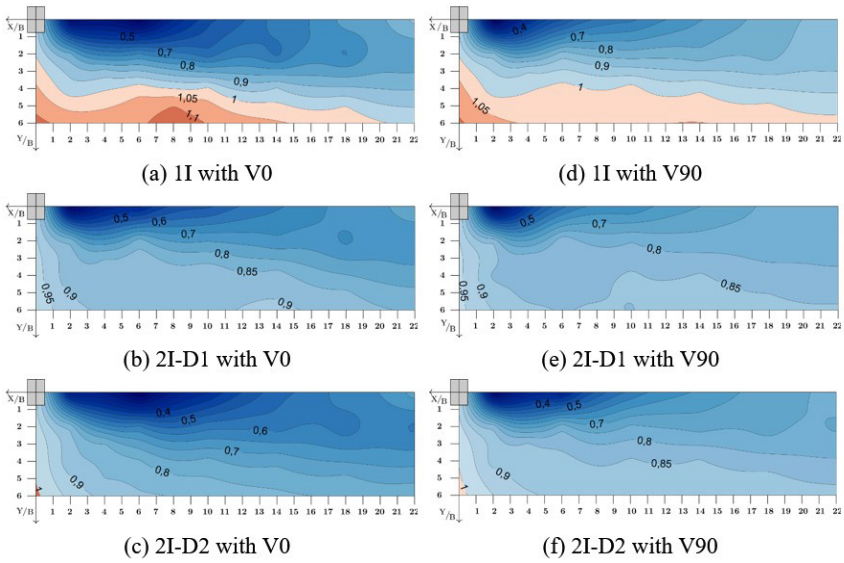

Figure 6. IFs contour plots of mean along-wind force coefficients for C0.

The maps in Figure 7 show that there was an increase in the amplification area when the principal building was positioned at 90° (C90) for the three groups of interfering buildings, showing interference effects above 15%. This more intense amplification occurs due to the lower drag force acting on the principal building isolated in this rotation, where any disturbance caused by the interfering building makes it possible to increase the load on the principal building.

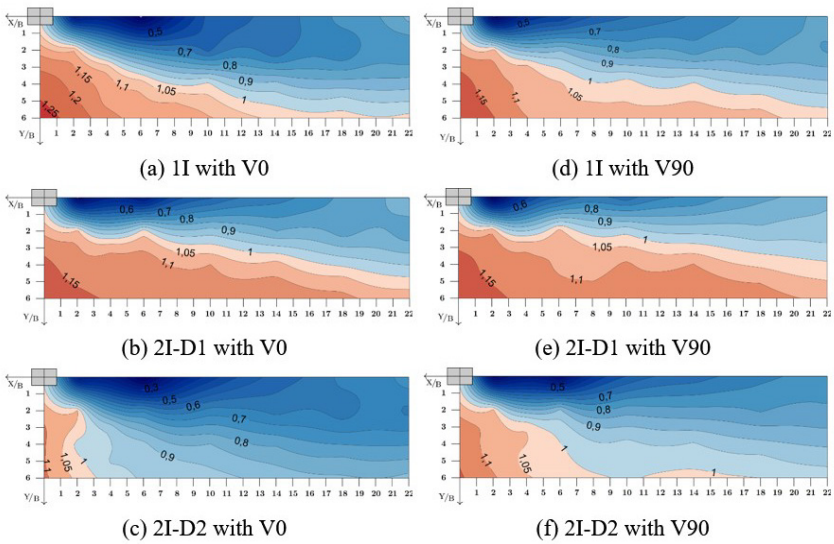

Figure 7. IFs contour plots of mean along-wind force coefficients for C90.

This influence is more evident in scenarios with interfering buildings at 0° (V0), since the approaching flow is more affected when compared to the scenarios with interfering buildings at 90° (V90), either by increasing turbulence or by generating more intense vortex shedding.

3.1.2 Across-wind force coefficients

The maps in Figure 8 show that in scenarios with the principal building at 0° (C0), the extent of protection caused by the interfering building is still high, especially in sets with V90. However, the effects of amplification are also found, except in Group 2 (2I-D1), where there was protection throughout the map area. This behavior reinforces the understanding of a greater change in the approaching flow on the analyzed building due to the vortex shedding, generated by the interfering building when its larger facade is normal to the incidence of the wind.

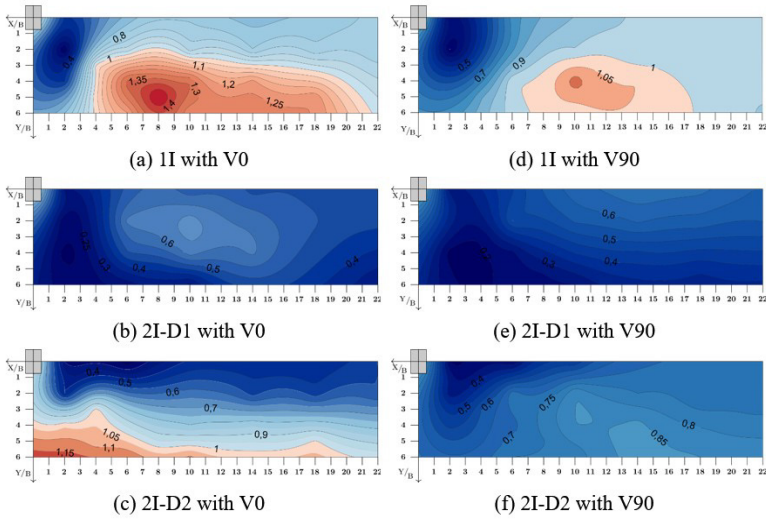

Figure 8. IFs contour plots of RMS across-wind force coefficients for C0.

This reduction in the shielding effect occurs as the fixed interfering building moves away from the principal building, especially at 0° rotation (V0), where the vortex shedding generated will affect the principal building on a larger scale.

In the maps of the IFs with the principal building at 90° (C90), Figure 9, it was observed that the amplification area covers practically all of these scenarios. The IF values range from 1.50 to values greater than 2.0 for the interfering buildings at 0° (V0) and from 1.15 to values greater than 1.50 for the interfering buildings at 90° (V90), similar to what was found by Zu and Lam [20], despite the differences in the parameters analyzed. It is noteworthy that the scenarios with V0 have a greater amplification due to the more intense disturbance of the approaching flow on the analyzed building, resulting in the formation of larger vortexes.

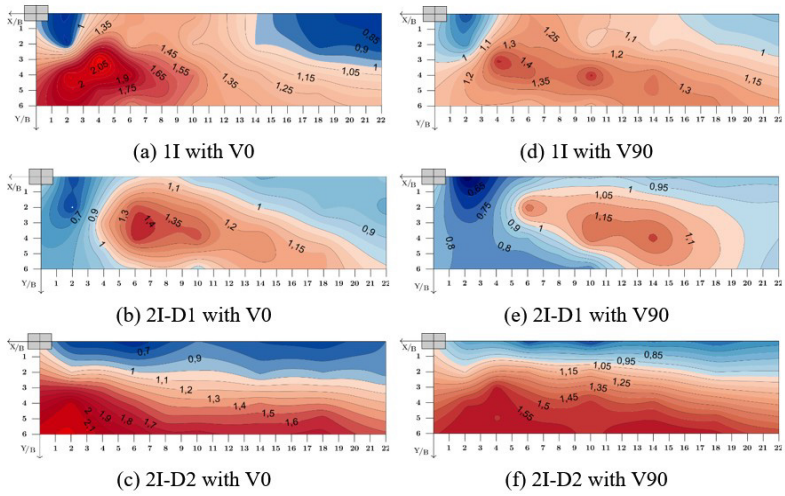

Figure 9. IFs contour plots of RMS across-wind force coefficients for C90.

Importantly, Group 2 (2I-D1) resulted in more extensive areas of protection, while Group 3 (2I-D2) resulted in more extensive areas of amplification, which differs from the mean along-wind force presented above. Once again, it is observed that the configurations with an interfering building at 0° (V0) present higher amplification due to the more intense interference in the approaching flow, resulting in the formation of larger vortex shedding.

3.1.3 Torsion moment coefficients

Through the maps of the IFs at the torsion moment of scenarios with the principal building at 0° (C0) in Figure 10, it was evident that the protection provided by the interfering buildings was significant, especially in the presence of the

second interfering building. However, amplification effects are observed in situations of the Group 1 with the interfering building at 0° (V0), indicating that in this type of scenario the turbulence generated by the interfering building increases the fluctuations with greater eccentricities.

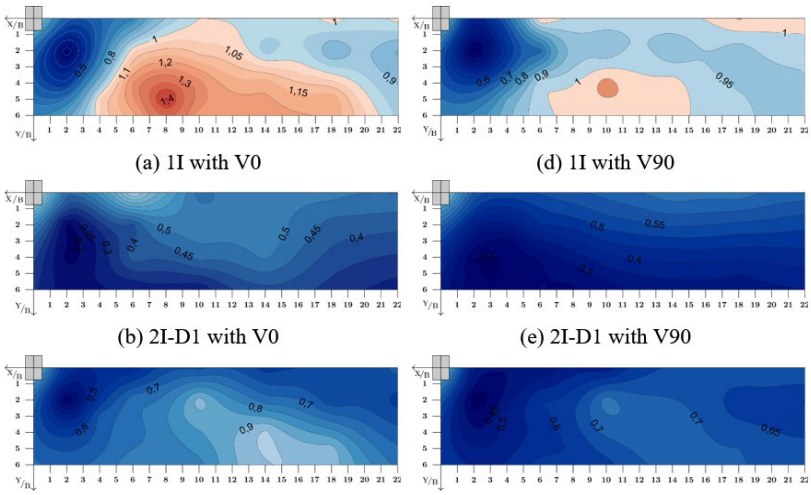

(a) 1I with V0 (d) 1I with V90

(b) 2I-D1 with V0 (e) 2I-D1 with V90

(c) 2I-D2 with V0 (f) 2I-D2 with V90

Figure 10. IFs contour plots of RMS torsion moment coefficients for C0.

In Figure 11, the amplification area on the maps in scenarios with the principal building at 90° (C90) occupies the maps almost entirely in the three interference groups. These high values indicate that the torsion fluctuations have a significant sensitivity to the turbulence generated by the interfering buildings when the analyzed building has the smaller facade normal to the incidence of wind. Again, it is noted that the sets with V0 have higher amplification relative to the sets with V90.

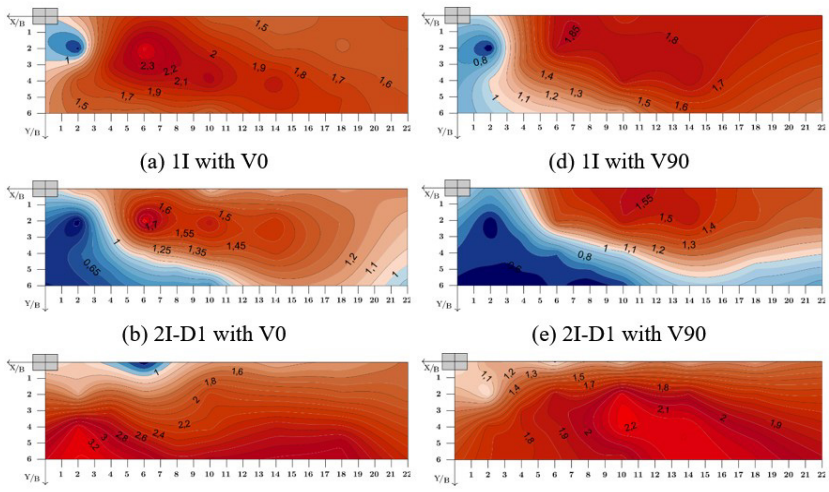

(a) 1I with V0 (d) 1I with V90

(b) 2I-D1 with V0 (e) 2I-D1 with V90

(c) 2I-D2 with V0 (f) 2I-D2 with V90

Figure 11. IFs contour plots of RMS torsion moment coefficients for C90.

Once again, the scenarios in which the principal building is positioned at 90° (C90) showed higher IFs compared to the sets with C0. This amplification of fluctuations suggests that situations with C90 are susceptible to resonant phenomena, even when there is a second interfering building, especially when this building is at a greater distance from the principal building.

3.2 Effects of Terrain Roughness

To facilitate a quantitative understanding of the results obtained in the IFs maps, in addition to comparing the results obtained for the roughness $p = 0.23$, available at Lavôr et al. [16], the graphs in Figures 12-14 show the percentage

distribution $p(\%)$ of the IFs for the three interference groups, taking into account the sets of relative rotation of the buildings with the highest amplifications.

Regarding the graphs in Figure 12, it can be seen that the amplification area in scenarios with the principal building at 0° (C0), as shown in Figures 12a and 12b, is approximately 6% with p = 0.11, with all of this area contained in Group 1 (1I), and approximately 11% with p = 0.23, with most of this area (94%) contained in Group 1 (1I).

The amplification area in scenarios with the principal building at 90° (C90), as shown in Figures 12c and 12d, is approximately 33% with p = 0.11, with 55% of this area contained in Group 2 (2I-D1) and 33% in Group 1 (1I), and approximately 33% with p = 0.23, with 56% of this area contained in Group 2 (2I-D1) and 32% in Group 1 (1I).

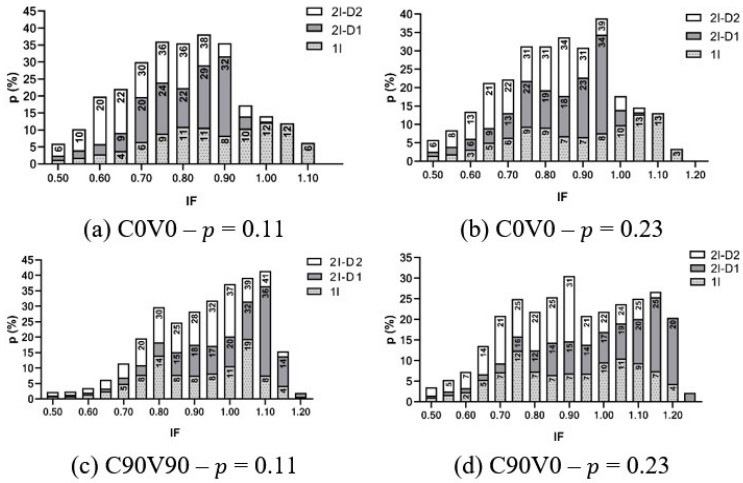

(a) C0V0 – p = 0.11 (b) C0V0 – p = 0.23

(c) C90V90 – p = 0.11 (d) C90V0 – p = 0.23

Figure 12. IFs percentage distribution of mean along-wind force coefficients.

As observed by Xie and Gu [13], the influence that roughness exerted on the along-wind force in the static analysis with one or two interfering buildings caused more significant protection effects in less rough terrain (p = 0.11), whereas rougher terrain (p = 0.23) resulted in more important amplifications.

The graphs in Figure 13 show that the amplification area in scenarios with the principal building at 0° (C0), as in Figures 13a and 13b is approximately 17% with p = 0.11, with most of this area (77%) contained in Group 1 (1I), and approximately 21% with p = 0.23, with most of this area (70%) contained in Group 1 (1I).

The amplification area in scenarios with the principal building at 90° (C90), as shown in Figures 13c and 13d, is approximately 61% with p = 0.11, with 39% of this area contained in Group 1 (1I) and 25% in Group 2 (2I-D1), and approximately 87% with p = 0.23, with 36% of this area contained in Group 2 (2I-D1) and 33% in Group 1 (1I).

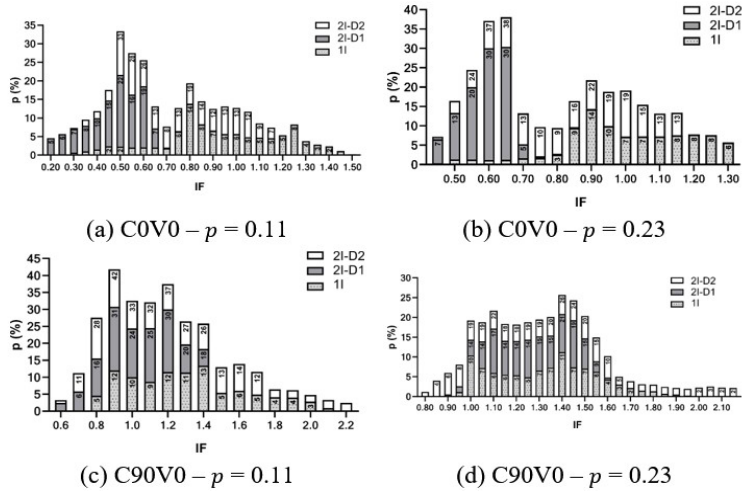

(a) C0V0 – p = 0.11 (b) C0V0 – p = 0.23

(c) C90V0 – p = 0.11 (d) C90V0 – p = 0.23

Figure 13. IFs percentage distribution of RMS across-wind force coefficients.

Similar results, both in the IFs locations and magnitudes, were found by Xie and Gu [21], where important alterations in the across-wind responses were also found when a second interfering building was present.

The graphs in Figure 14 show that the amplification area in scenarios with the principal building at 0° (C0), as in Figures 14a and b, is approximately 15% with $p = 0.11$, with all this area contained in Group 1 (1I), and approximately 15% with $p = 0.23$, with all this area also contained only in Group 1 (1I).

The amplification area in scenarios with the principal building at 90° (C90), as shown in Figures 14c and d, is approximately 91% with $p = 0.11$, with 39% of this area contained in Group 2 (2I-D1) and 36% in Group 1 (1I), and approximately 61% with $p = 0.23$, with 50% of this area contained in Group 1 (1I) and 47% in Group 2 (2I-D1).

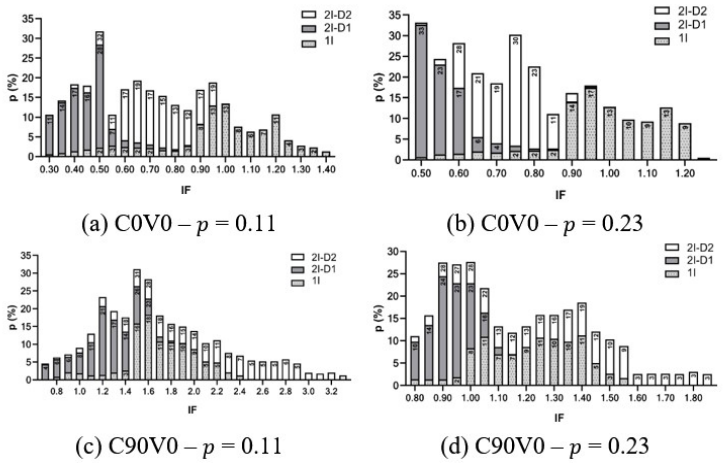

Figure 14. IFs percentage distribution of RMS torsion moment coefficients.

It is notable that, in contrast to the loads analyzed above, the fluctuations of the torsion moment with the principal building at 90° (C90) were considerably affected by the terrain roughness, as seen in Mara et al. [14].

3.3 Normative Generalizations

In addition to the complexity involved in the phenomenon of aerodynamic interference, a large number of the studies that address the subject have presented results with large inconsistencies between them. Khanduri et al. [22] concluded that these discrepancies could be minimized if researchers acted more systematically, proposing a general set of guidelines that could be practically adopted.

Such problems directly affect the quantitative standardization of interference effects, conditioning the standards and engineering codes to directly suggest tests in a wind tunnel, in which the interference conditions are reproduced in a particular way. However, indications of numerical values for the interference factors can be found, serving as preliminary estimates for design, in the standards IS 875 [23], AIJ [24], GB 50009 [25] and NBR 6123 [17].

The Indian standard IS 875 [23] presents the IF values through zones delimited by coordinates according to the smaller dimension of the analyzed building, as shown in Figure 15. The code does not specify the direction of the response to which the IFs should be applied, and the presented map suggests that these factors are valid only for the wind incidence against the smaller facade of the analyzed building, since there is no description of the wind direction in the text.

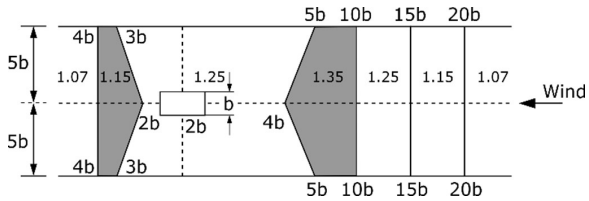

Figure 15. Interference zones of the Indian standard. Adapted from IS 875 [23].

The Chinese standard GB 50009 [25] presents the maps as contour lines, separating the maps with IFs of the along-wind and across-wind forces, as shown in Figure 16. The maps are valid for buildings with a square base and delimited by coordinates according to the width of the analyzed building. Unlike the Indian standard, the maps are available in the comments of the Chinese standard but not in its main body.

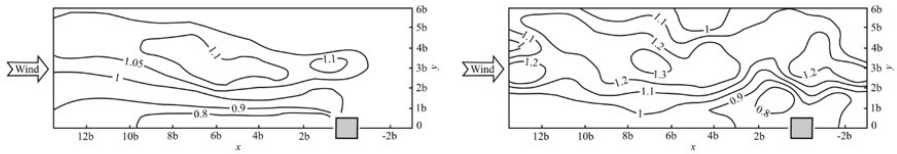

(a) IFs in the along-wind force (b) IFs in the across-wind force

Figure 16. Interference factors of the Chinese standard. Adapted from the comments in GB 50009 [25].

The Japanese standard AIJ [24] considers, in addition to the use of maps with contour lines to represent the IFs and distinguish the along-wind and the across-wind directions, the indication of IFs values according to some terrain roughness, as shown in Figure 17. The standard makes it clear that this indication is limited to a square-based interference building with the same size as the analyzed one, for a wind velocity range between 40 and 60 m/s.

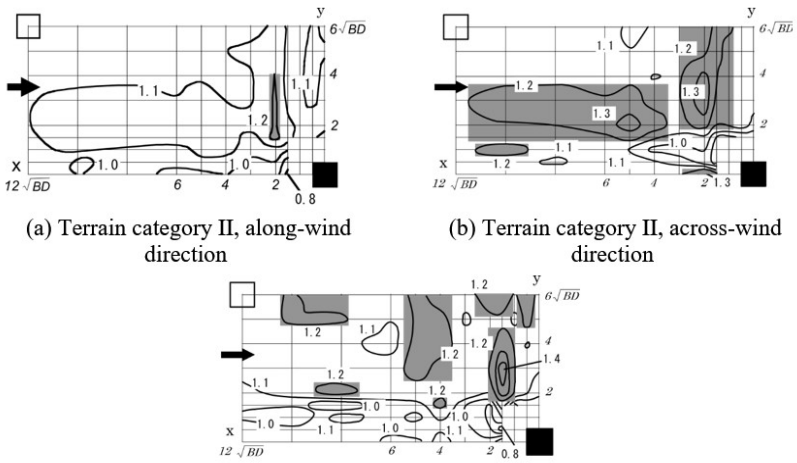

(a) Terrain category II, along-wind direction (b) Terrain category II, across-wind direction

(c) Terrain category IV, across-wind direction

Figure 17. Interference factors of the Japanese standard. Adapted from AIJ [24].

Among the standards mentioned, the Brazilian standard is the only one that does not provide a reference of the interference effects through an interference factor map, and like the Indian standard, it does not specify in which direction to apply the suggested values. Thus, to clarify the recommendations of NBR 6123 [17], an IFs map was drawn by applying the high-rise building model of this study to the prescriptions of the standard, as shown in Figure 18.

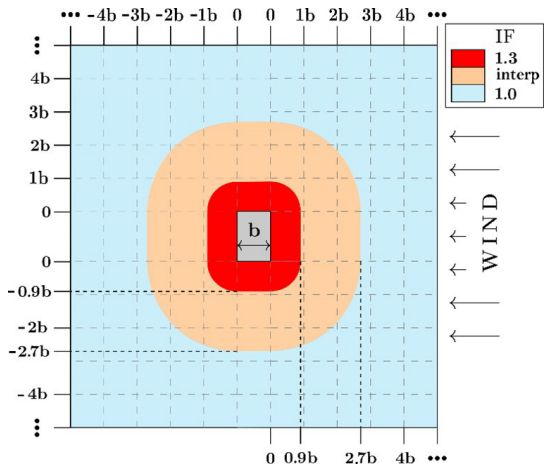

Figure 18. Interference factors of the Brazilian standard.

The interference factors, applicable to the mean pressure coefficients, are determined through the following relationships in Equation 8.

$$\frac{s}{d^*} \leq 1.0 \rightarrow IF = 1.3$$
$$\frac{s}{d^*} \geq 3.0 \rightarrow IF = 1.0 \quad (8)$$

where s is the distance between the analyzed building and the interfering one; and d^* is defined by the smallest value between b and $1/2 \cdot (a^2 + b^2)^{1/2}$, where a and b are, respectively, the larger and smaller side of the cross-section of the analyzed building. Intermediate values of s/d^* can be linearly interpolated. It is important to note that the standard does not mention whether these values refer to positions upstream, downstream or in both positions from the analyzed building.

Applying these relationships to the building analyzed in this study, one observes the degree of lag of these results in relation to those found here, and in most studies on the subject, with regard to the location and dimensions of the amplification zones of the interference factors. Since the value of IF = 1.3 is consistent with the amplifications presented by the previous studies and standards, but in areas further away from the analyzed building and with greater extensions, as analyzed by Vieira et al. [26].

Clearly, the three standards have limitations in their prescriptions, such as the wind angle of incidence, the quantity and shape of the buildings, the direction of the loads, the terrain roughness and the nature of the analysis, where in the case of a dynamic analysis, even more parameters such as the wind velocity and the dynamic characteristics of the structure are given. Therefore, quantifying interference effects through codes and standards is still impractical due to the complexity of the multiple parameters involved.

4 CONCLUSIONS

The interference caused by buildings was explored through a series of tests in a wind tunnel using the technique of synchronized pressure measurement in a rigid model. The effects of distance and number of interfering buildings, wind incidence angle, relative rotation of buildings and terrain roughness were evaluated. In addition, normative prescriptions on the interference effects were presented and evaluated. Based on an analysis of the results, the conclusions can be summarized as follows:

1. From the maps of the interference factors of the aerodynamic coefficients with a roughness of p = 0.11, it was observed that the largest extension of the amplification zones occurred in scenarios in which the wind hit the smaller facade of the principal building (C90) and on the larger facade of the interfering building (V0), i.e., in the C90V0 sets. In general terms, when performing the static analysis, it was observed that the shielding effect is a dominant phenomenon in most cases studied when there is wind interference.
2. For the along-wind force coefficient, in Groups 2 and 3, i.e., in the presence of the second interfering building, there was protection with C0 and amplification with C90, especially in the presence of "D1", the fixed interfering building closest to the principal building. The same occurred with the across-wind force coefficient and the torsion moment; however, it was the fixed interfering building "D2", farthest from the principal building, that caused the greatest amplification.
3. The increase in the terrain roughness, changing the power law exponent from p = 0.11 to p = 0.23, did not produce significant divergences in the along-wind and across-wind forces on the building. Even when presenting interference factors with higher magnitudes in rougher terrain, the variations were minimal.
4. The RMS torsion moment coefficient was more sensitive to changes in the wind flow, where the low increase in the level of terrain roughness, from p = 0.11 to p = 0.23, resulted in significant differences in the interference effects when compared to the other analyzed loads.
5. The obtained results confirmed the complex nature of the phenomenon, as mentioned in other studies. However, the magnitude of these results was consistent with the values established by the aforementioned standards. This differs from the Brazilian standard only in the coordinates of the critical effects, as this standard clearly lags in this parameter, requiring revision.

Due to both the complexity of the phenomenon and the more qualitative level of its current understanding, there is a need for more experimental tests, numerical studies, and implementation and training of neural networks and artificial intelligence, all integrated with each other. Thus, there will be more solid foundations for normative generalization of interference effects.

ACKNOWLEDGEMENTS

We acknowledge for the financial support by CAPES Brazil and the joint support by the Universidade de Brasília, PECC Postgraduate Program, Universidade Federal do Rio Grande do Sul and LAC Wind Tunnel team.

REFERENCES

[1] J. W. Saunders and W. H. Melbourne, “Buffeting effects of upstream buildings,” in *Proc. Fifth Int. Conf.*, Fort Collins, CO, USA, 1980, pp. 593–606. http://dx.doi.org/10.1016/B978-1-4832-8367-8.50059-0.

[2] D. M. Sykes, "Interference effects on the response of a tall building model," *J. Wind Eng. Ind. Aerodyn.*, vol. 11, no. 1–3, pp. 365–380, 1983, http://dx.doi.org/10.1016/0167-6105(83)90114-9.

[3] J. Blessmann, "Buffeting effects on neighbouring tall buildings," *J. Wind Eng. Ind. Aerodyn.*, vol. 18, no. 1, pp. 105–110, 1985, http://dx.doi.org/10.1016/0167-6105(85)90077-7.

[4] P. A. Bailey and K. C. S. Kwok, "Interference excitation of twin tall buildings," *J. Wind Eng. Ind. Aerodyn.*, vol. 21, no. 3, pp. 323–338, 1985, http://dx.doi.org/10.1016/0167-6105(85)90043-1.

[5] A. Kareem, "The effect of aerodynamic interference on the dynamic response of prismatic structures," *J. Wind Eng. Ind. Aerodyn.*, vol. 25, no. 3, pp. 365–372, 1987, http://dx.doi.org/10.1016/0167-6105(87)90028-6.

[6] Y. Taniike, "Interference mechanism for enhanced wind forces on neighboring tall buildings," *J. Wind Eng. Ind. Aerodyn.*, vol. 42, no. 1–3, pp. 1073–1083, 1992, http://dx.doi.org/10.1016/0167-6105(92)90114-P.

[7] M. Gu, Z. N. Xie, and P. Huang, "Along-wind dynamic interference effects of tall buildings," *Adv. Struct. Eng.*, vol. 8, no. 6, pp. 623–636, 2005, http://dx.doi.org/10.1260/136943305776318400.

[8] F. M. Fang, C. Y. Chung, Y. C. Li, W. C. Liu, and P. K. Lei, "The across-wind response of the downwind prism in a twin-prism system with a staggered arrangement," *Wind Struct.*, vol. 17, no. 3, pp. 245–262, 2013, http://dx.doi.org/10.12989/was.2013.17.3.245.

[9] F. Wang, Y. Tamura, and A. Yoshida, "Interference effects of a neighboring building on wind loads on scaffolding," *J. Wind Eng. Ind. Aerodyn.*, vol. 125, pp. 1–12, 2014, http://dx.doi.org/10.1016/j.jweia.2013.11.009.

[10] Y. Lo, Y. Li, and Y. Kim, "Downstream interference effect of low-scruton-number high-rise buildings under turbulent boundary layer flow," *J. Wind Eng. Ind. Aerodyn.*, vol. 198, pp. 104101, 2020, http://dx.doi.org/10.1016/j.jweia.2020.104101.

[11] M. N. Reis, T. F. A. Lavôr, J. C. Pantoja, and J. L. V. Brito, "Numerical-experimental study of neighboring wind effects on tall buildings related to serviceability via reliability," *Rev. IBRACON Estrut. Mater.*, vol. 15, no. 5, e15507, 2022, http://dx.doi.org/10.1590/s1983-41952022000500007.

[12] T. Wang, K. C. S. Kwok, Q. Yang, Y. Tian, and B. Li, "Experimental study on proximity interference induced vibration of two staggered square prisms in turbulent boundary layer flow," *J. Wind Eng. Ind. Aerodyn.*, vol. 220, no. 104865, pp. 104865, 2022, http://dx.doi.org/10.1016/j.jweia.2021.104865.

[13] Z. N. Xie and M. Gu, "Mean interference effects among tall buildings," *Eng. Struct.*, vol. 26, no. 9, pp. 1173–1183, 2004, http://dx.doi.org/10.1016/j.engstruct.2004.03.007.

[14] T. G. Mara, B. K. Terry, T. C. E. Ho, and N. Isyumov, "Aerodynamic and peak response interference factors for an upstream square building of identical height," *J. Wind Eng. Ind. Aerodyn.*, vol. 133, pp. 200–210, 2014, http://dx.doi.org/10.1016/j.jweia.2014.06.010.

[15] W. Kim, Y. Tamura, and A. Yoshida, "Interference effects on aerodynamic wind forces between two buildings," *J. Wind Eng. Ind. Aerodyn.*, vol. 147, pp. 186–201, 2015, http://dx.doi.org/10.1016/j.jweia.2015.10.009.

[16] T. F. A. Lavôr, J. L. V. Brito, and A. M. Loredo-Souza, "Interference effects mapping on the static wind loading of a tall building," *Lat. Am. J. Solids Struct.*, vol. 20, no. 3, e484, 2023, http://dx.doi.org/10.1590/1679-78257330.

[17] Associação Brasileira de Normas Técnicas, *Forças Devidas ao Vento em Edificações*, ABNT NBR 6123, 2023.

[18] Y. Hui, Y. Tamura, and Q. Yang, "Analysis of interference effects on torsional moment between two high-rise buildings based on pressure and flow field measurement," *J. Wind Eng. Ind. Aerodyn.*, vol. 164, pp. 54–68, 2017, http://dx.doi.org/10.1016/j.jweia.2017.02.008.

[19] Y. Hui, A. Yoshida, and Y. Tamura, "Interference effects between two rectangular section high-rise buildings on local peak pressure coefficients," *J. Fluids Structures*, vol. 37, pp. 120–133, 2013, http://dx.doi.org/10.1016/j.jfluidstructs.2012.11.007.

[20] G. B. Zu and K. M. Lam, "Across-wind excitation mechanism for interference of twin tall buildings in staggered arrangement," *J. Wind Eng. Ind. Aerodyn.*, vol. 177, pp. 167–185, 2018, http://dx.doi.org/10.1016/j.jweia.2018.04.019.

[21] Z. N. Xie and M. Gu, "Across-wind dynamic response of high-rise building under wind action with interference effects from one and two tall buildings," *Struct. Des. Tall Spec. Build.*, vol. 18, no. 1, pp. 37–57, 2009, http://dx.doi.org/10.1002/tal.393.

[22] A. C. Khanduri, T. Stathopoulos, and C. Bédard, "Wind-induced interference effects on buildings – a review of the state-of-the-art," *Eng. Struct.*, vol. 20, no. 7, pp. 617–630, 1998, http://dx.doi.org/10.1016/S0141-0296(97)00066-7.

[23] Bureau of Indian Standard, *Design Loads (Other than Earthquake) for Buildings and Structures-Code of Practice,* IS 875 (Part 3), 2015.

[24] Architectural Institute of Japan, *Recommendations for Loads on Buildings – Chapter 6 – Wind Loads*, Japan: AIJ, 2015.

[25] National Standard of the People's Republic of China, *Load Code for the Design of Building Structures*, GB 50009, 2012.

[26] G. S. Vieira, J. L. V. Brito, and A. M. Loredo-Souza, "Experimental study on the interference intensity produced by the presence of neighboring buildings in the wind action in a tall building," *Rev. IBRACON Estrut. Mater.*, vol. 11, no. 5, pp. 1036–1052, 2018, http://dx.doi.org/10.1590/s1983-41952018000500008.

Author contributions: TFAL: conceptualization, methodology, writing, formal analysis, development of numerical procedures and experimental tests; JLVB: conceptualization, methodology and writing review; AMLS: conceptualization, supervision.

Editors: Sergio Hampshire de Carvalho Santos, Daniel Carlos Taissum Cardoso.